1968-01-01

Ion Acoustic Wave Dispersion in a Highly Ionized Argon Plasma In a Magnetic Field.

Levin, R.R.; Oleson, N.L.

Journal Name: Phys. Fluids, 11: 2251-8(Oct. 1968).; Other Information: Orig. Receipt Date: 31-DEC-68
http://hdl.handle.net/10945/57779

scalars. This allows truncation of the set of moments of the Boltzmann equation after the first two moments, which are the equation of continuity and the momentum transfer equation, respectively. These equations are combined with the plasma equation of state. Assumption of the azimuthal and longitudinal forms of the wave behavior allows the resulting partial differential equation to be reduced to an ordinary differential equation involving only the radial behavior. This equation is solved in series form and yields the dispersion relation when the boundary condition is inserted.

II. THEORETICAL ASPECTS

The ions and electrons are assumed to move in phase due to the strong electrostatic restoring forces so that the instantaneous ion and electron densities are approximately equal. Although the Coulomb interaction is the mechanism by which these waves propagate, there is no macroscopic electric field associated with the waves.

Since the electron temperature greatly exceeds the ion temperature and the Debye length is very small, the number of positive ions capable of causing Landau damping is negligible.[9] Similarly, the thermal speeds of the electrons are much greater than the phase velocities and as a result the electrons see these waves as being quasistatic and do not contribute any Landau damping. Hence Landau damping due to both ions and electrons can be ignored.

In the following derivation the quantities $\mathbf{W}$, $\mathbf{B}_0$, T_e, and T_i are assumed to be functions neither of position nor of time: $\mathbf{W}$ is the equilibrium ion drift velocity, $\mathbf{B}_0$ is the axial static magnetic field strength, T_e is the electron temperature, and T_i is the ion temperature.

If the electron and ion pressures are considered to be scalars, the momentum transfer equation for the ions under the influence of the perturbation is

$$-\frac{1}{M}\nabla(P_e + P_i + p_e + p_i)$$
$$= \left(\frac{\partial}{\partial t} + (\mathbf{v} + \mathbf{W})\cdot\nabla\right)[(N + n)(\mathbf{v} + \mathbf{W})]$$
$$+ (N + n)(\mathbf{v} + \mathbf{W})\nu - \Omega(N + n)(\mathbf{v} + \mathbf{W})\times\hat{z}, \quad (1)$$

where P_e is the equilibrium electron pressure, P_i is the equilibrium ion pressure, p_e is the electron pressure perturbation, p_i is the ion pressure perturbation, v is the ion velocity induced by the wave, N is the equilibrium ion density, n is the ion density perturbation, ν is the ion–neutral collision frequency, Ω is the ion cyclotron frequency $= eB_0/M$, and $\hat{z}$ is the unit vector in the axial direction.

If one subtracts the similar equation for the ions corresponding to the unperturbed plasma column and considers the perturbations to be small, the resulting equation can be partially linearized to the first order of small quantities, yielding

$$-\frac{1}{M}\nabla(p_e + p_i) = N\frac{\partial\mathbf{v}}{\partial t} + (\mathbf{v} + \mathbf{W})\frac{\partial n}{\partial t}$$
$$+ (\mathbf{v}\cdot\nabla)(N + n)(\mathbf{v} + \mathbf{W})$$
$$+ (\mathbf{W}\cdot\nabla)(N\mathbf{v} + n\mathbf{v} + n\mathbf{W})$$
$$+ \nu(N\mathbf{v} + n\mathbf{W}) - \Omega N\mathbf{v}\times\hat{z}. \quad (2)$$

Solutions of this equation in the form

$$\exp[i(\mu\theta + kz - \omega t)]$$

are sought, and $\mathbf{W}$ is assumed to be in the $\hat{z}$ direction so that $W\cdot\nabla \rightarrow W\partial/\partial z$. The angular frequency ω is assumed to be real and k and μ, the longitudinal and azimuthal wavenumbers, respectively, are complex. The radial form of the density perturbation is not specified at this point.

If the expression $(\mathbf{v}\cdot\nabla)\ (N + n)\ (\mathbf{v} + \mathbf{W})$ is linearized to the first order of small quantities, Eq. (2) can be put into the form

$$-\frac{1}{M}\nabla(p_e + p_i)$$
$$= -i\omega N\mathbf{v} - i\omega n\mathbf{W} + Wv_r\left(\frac{\partial N}{\partial r}\right)\hat{z}$$
$$+ ikW(N\mathbf{v} + n\mathbf{W}) + \nu(N\mathbf{v} + n\mathbf{W})$$
$$- \Omega N v_\theta\hat{r} + \Omega N v_r\hat{\theta}, \quad (3)$$

where $\mathbf{v} = v_r\hat{r} + v_\theta\hat{\theta} + v_z\hat{z}$; $\hat{r}$, $\hat{\theta}$, and $\hat{z}$ being unit vectors in the r, θ, and z directions, respectively. By solving Eq. (3) for the quantities Nv_θ and Nv_r and taking the divergence of $Nv_\theta\hat{r} - Nv_r\hat{\theta}$, one finds that

$$\nabla\cdot(Nv_\theta\hat{r} - Nv_r\hat{\theta}) = \frac{\Omega}{M}\left[\frac{\partial^2}{\partial r^2} + \frac{1}{r}\frac{\partial}{\partial r} - \frac{\mu^2}{r^2}\right]$$
$$\cdot\frac{(p_e + p_i)}{(i\omega - ikW - \nu)^2 + \Omega^2}. \quad (4)$$

If volume recombination and ionization are neglected, the equation of continuity for the ions is given by

$$\nabla\cdot(N + n)(\mathbf{v} + \mathbf{W}) = -\frac{\partial}{\partial t}(N + n) = i\omega n. \quad (5)$$

[9] B. Fried, in *Plasma Physics in Theory and Application*, W. Kunkel, Ed. (McGraw-Hill Book Company, New York, 1966), p. 80.

If use is made of Eqs. (4) and (5) and the relation $\nabla^2 p = KT\nabla^2 n$, the divergence of Eq. (3) becomes

$$(c^2 + C^2)\left\{\left[\frac{\partial^2 n}{\partial r^2} + \frac{1}{r}\frac{\partial n}{\partial r} - \frac{\mu^2}{r^2}n\right] \cdot \left[\frac{(i\omega - ikW - \nu)^2}{(i\omega - ikW - \nu)^2 + \Omega^2}\right] - k^2 n\right\} + (c^2 + C^2)\frac{W}{N}\frac{\partial N}{\partial r} \cdot \left[\frac{ik(\partial n/\partial r)(i\omega - ikW - \nu) + (\mu/r)\Omega kn}{(i\omega - ikW - \nu)^2 + \Omega^2}\right] + \omega^2 n - \omega kWn - i\omega\nu n = 0, \quad (6)$$

where

$$c^2 = \frac{KT_e}{M}, \qquad C^2 = \frac{KT_i}{M},$$

and radial invariance of T_e and T_i have been assumed.

Equation (6) would be directly reducible to Bessel's equation of order μ if $\partial N/\partial r$ were equal to zero (uniform radial density distribution in the unperturbed column). This, however, is not the case in the present investigation. The mean free path for ion–neutral collisions is greater than 1 m while the ion gyroradius is of the order of 10^{-3}m. Up to several gyroradii away from the beam axis, the analysis of Pfirsch and Biermann[10] predicts that for a Maxwellian velocity distribution and a Gaussian distribution of the guiding centers of the charged particles there will be a Gaussian density profile. Probe measurements by Gall and Oleson[11] have shown that the radial density profile of N in argon is represented by a Gaussian, at least to a good approximation. Thus,

$$N = N_0 e^{-\delta^2 r^2},$$

so that

$$\frac{1}{N}\frac{\partial N}{\partial r} = -2\,\delta^2 r$$

and Eq. (6) becomes

$$s^2\frac{\partial^2 n}{\partial s^2} + \frac{\partial n}{\partial s}\left[s - \frac{2s^3\,\delta^2 kW}{(\omega - kW + i\nu)\lambda^2}\right] + n(s^2 - \mu^2) = 0, \quad (7)$$

where $s \equiv \lambda r$ and

$$\lambda^2 \equiv \left[\frac{\Omega^2}{(\omega - kW + i\nu)^2} - 1\right] \cdot \left[k^2 - \frac{\omega(\omega - kW + i\nu)}{c^2 + C^2}\right] + \frac{2\mu\,\delta^2\Omega kW}{(\omega - kW + i\nu)^2}.$$

If a solution of the form

$$n = n_0 s^\rho \sum_{i=0}^{\infty} a_i s^i, \qquad a_0 \neq 0$$

is assumed and inserted into Eq. (7), the following recursion relation results:

$$a_{2i} = \frac{g^i \Gamma[j + \frac{1}{2}|\mu| - (1/2g)]}{2^{|\mu|}2^i j!\,(j + |\mu|)!\,[\frac{1}{2}|\mu| - (1/2g)]}$$

and

$$\rho = |\mu|,$$

where a_0 has been chosen as $(2^{|\mu|}\,|\mu|\,!)^{-1}$. Thus, the solution of Eq. (7) is

$$n(s) = n_0 \exp[i(\mu\theta + kz - \omega t)] \cdot \sum_{i=0}^{\infty} \frac{g^i \Gamma(j + b)s^{[|\mu| + 2j]}}{2^{|\mu|}2^i j!\,(j + |\mu|)!\,\Gamma(b)}, \quad (8)$$

where

$$b \equiv \frac{|\mu|\,g - 1}{2g},$$

$$g \equiv \frac{2\,\delta^2 kW}{(\omega - kW + i\nu)\lambda^2}.$$

Equation (8) reduces to the Bessel function J_μ when $g = 0$ (uniform density in the unperturbed column). For this case the dispersion relation assumes the simple form $\lambda l = 2.405$ ($\mu = 0$) where the boundary condition has been imposed that $r = l$ corresponds to the radial position at which the perturbation becomes negligibly small. The validity of this type of boundary condition was confirmed by probe measurements which is discussed in the following section. Consequently, no assumption need be made concerning the existence of either a pressure or velocity node at the plasma boundary.

Evidence is also presented in the next section that only the $\mu = 0$ mode is excited. For this case the dispersion relation for $g \neq 0$ is found to be

$$\sum_{i=0}^{\infty} \frac{g^i \Gamma[j - (1/2g)](\lambda^2 l^2)^i}{2^i j!\,j!\,\Gamma[-(1/2g)]} = 0, \quad (9)$$

where now

$$g \equiv \frac{2\,\delta^2 kW}{(\omega - kW + i\nu)\lambda^2},$$

[10] D. Pfirsch and L. Biermann, Z. Naturforsch. **15a**, 14 (1960).

[11] D. M. Gall and N. L. Oleson, in *Proceedings of the Seventh International Conference on Phenomena in Ionized Gases*, B. Perovic and D. Tosic, Eds. (Gradevinska Knjiga, Beograd, Yugoslavia, 1966), p. 31.

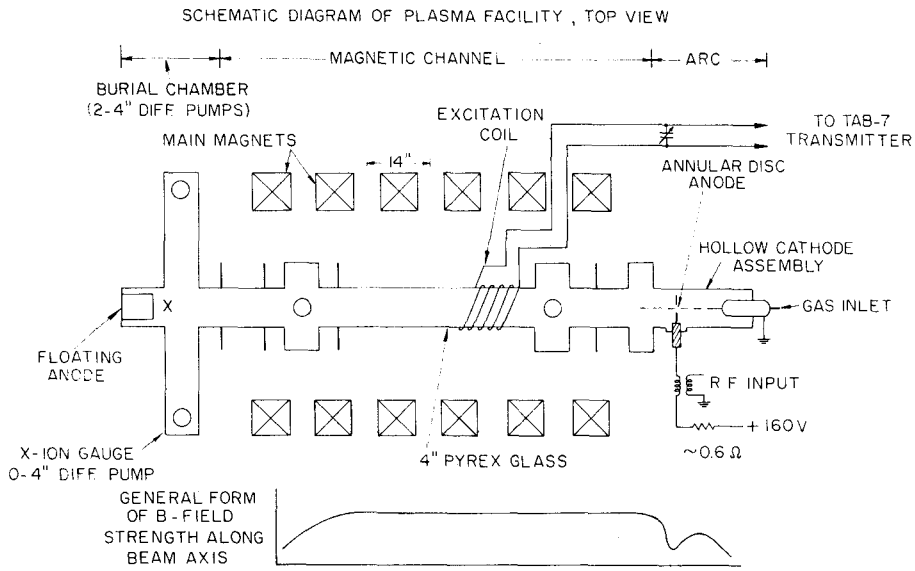

FIG. 1. Schematic diagram of top view of plasma facility.

$$\lambda^2 \equiv \left[\frac{\Omega^2}{(\omega - kW + i\nu)^2} - 1\right] \cdot \left[k^2 - \frac{\omega(\omega - kW + i\nu)}{c^2 + C^2}\right].$$

Equation (9) was compared to the experimental data by a least-squares direct search computer program on a CDC 1604.

III. EXPERIMENTAL ARRANGEMENT

A schematic illustration of the steady-state plasma facility appears in Fig. 1. The plasma is produced by a hollow cathode discharge, which has been extensively investigated by Lidsky *et al.*[12] Neutral argon gas is supplied through a micrometer valve assembly to the hollow cathode. An rf voltage is supplied between the cathode and the first anode in order to ignite the arc. Once the arc has been struck, the discharge is self-sustaining, and the rf voltage is turned off. The plasma so produced drifts through the hole in the first anode and into the experimental tube. This section is a 3-m long Pyrex tube of inside diameter 10 cm. It is axially aligned with the confining magnetic channel to within 1 mm throughout the length of the experimental region. The magnetic field is uniform to within 5% along the machine axis. To achieve optimum operating conditions, the neutral gas pressure is regulated through the input feed micrometer valve assembly. Differential pumping of the neutral atoms by the diffusion pumps maintains a gas pressure during operation of approximately 3×10^{-5} Torr throughout the experimental region so that ionization is between 70% and 90%.

In order to excite the waves, a short rf coil was tightly wrapped around the Pyrex tube as shown in Fig. 1. The coil was the inductive arm of a parallel tank circuit which was tuned to resonance at the applied transmitter frequency. Direct measurement of the rf magnetic fields produced by this coil yielded values of from 125 to 195 G, depending on the output power of the Westinghouse TAB-7 transmitter. This magnetic perturbation was superimposed on the static axial magnetic field (which was varied from 800 to 2200 G).

Once generated, the waves were observed to propagate parallel to the static field in both directions. Only propagation antiparallel to the static field was investigated in detail. (One set of parallel propagation measurements was made for a static axial magnetic field of 1000 G; this allowed an independent determination of the ion drift velocity.)

Previous spectroscopic measurements[13] have established that virtually all the light emitted by the plasma is from excited neutral atoms. Therefore, the emitted light intensity at any point along the plasma column is directly dependent on the local electron density, and a photomultiplier tube can be used to detect the presence of the waves. The detection circuit schematic is shown in Fig. 2. The optical signal was fed to the 1P21 phototube through a 10-ft flexible optical fiber bundle. After filtering and amplification a Tektronix dual beam oscilloscope, Type 555, was used to display the detected signal and to

[12] L. M. Lidsky, D. J. Rose, S. D. Rothleder, and S. Yoshikawa, J. Appl. Phys. **33**, 2940 (1962).

[13] R. Booth and R. L. Kelly (private communication).

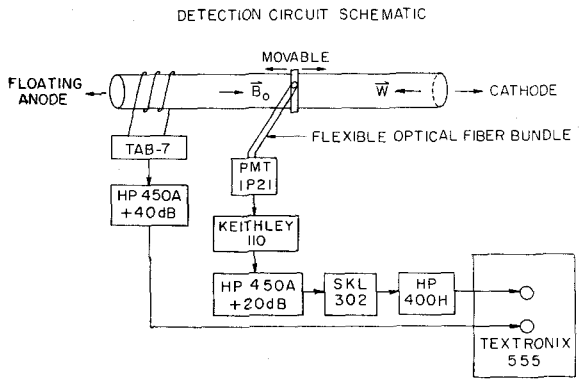

FIG. 2. Schematic of circuit for detecting ion acoustic waves.

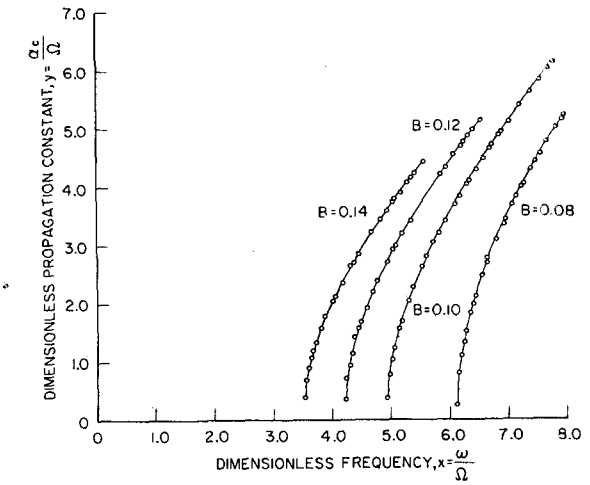

FIG. 3. Propagation number versus frequency. The circles are experimental points and the solid curves represent the dispersion relation using values of the five parameters (see text) giving the best fit. The parameter B is the axial magnetic field in webers per square meter.

compare it with a monitor signal taken directly from the transmitter. Both signals were subject to various phase delays (due to coupling into and out of the plasma, elements in the detector circuit, etc.), but comparison of the phases of the two signals gave the relative phase delay of the arriving signal. A measurement of the distance along the positive column between two axial positions of the optical fiber corresponding to the same phase of the observed signal yielded the wavelength of the propagating wave.

Langmuir type probes were inserted into the plasma in an attempt to detect the possible presence of the $\mu = 1, 2, 3$ modes. At maximum detection sensitivity no such waves were detected, consistent with the fact that the excitation mechanism had azimuthal symmetry, and modes other than $\mu = 0$ should not be present. Confirmation that the detected wave was actually the $\mu = 0$ mode was made by moving the probe radially from the plasma axis outward. The perturbation was observed to have a maximum at $r = 0$ (on the beam axis), decreasing monotonically as the probe was moved off the axis. Such behavior would only be consistent with the presence of the $\mu = 0$ mode as all higher modes would exhibit a null at $r = 0$. These measurements revealed no detectable perturbations beyond a distance of 15 mm from the beam axis. No standing waves were ever observed.

IV. ANALYSIS OF DATA

For a real angular frequency ω and a complex propagation number $k = \alpha + i\beta$, a set of data for a given axial magnetic field consists of α and β as functions of ω. Measurement of the wavelength by the procedure outlined in the previous section gives $2\pi/\alpha$. The damping increment β is obtainable from intensity measurement of the wave mode one wavelength apart. Then

$$\frac{I_1}{I_0} = \exp(\beta\,|z_1 - z_0|),$$

where

$$|z_1 - z_0| = \frac{2\pi}{\alpha}, \quad \text{or} \quad \frac{I_1}{I_0} = \exp\left[-\frac{2\pi\beta}{\alpha}\right],$$

from which β can be calculated directly. The entire set of data (that is, α and β vs ω) for a given field strength are then read into a direct search computation program which simultaneously adjusts the five parameters, W, ν, C, l, and δ, to find the dispersion function yielding the least-squares error when compared to the data. c is calculated using $T_e \approx 20$ eV as indicated by the data of Gall and Oleson.[11] In addition to performing this calculation, graphical displays were obtained for y vs x and z vs x (Figs. 3 and 4) where the variables have been reduced to the dimensionless quantities

$$x = \frac{\omega}{\Omega}, \qquad y = \frac{\alpha c}{\Omega}, \quad \text{and} \quad z = \frac{\beta c}{\Omega}.$$

The plotted circles represent the data points, and the continuous curve represents the dispersion relation using the values of the five parameters giving the best fit. The parameter appearing in the figures is the longitudinal static magnetic field $B_0(\mathrm{W/m^2})$.

Figures 5 and 6 show the behavior of the dimensionless phase velocity $(1/c)(\omega/\alpha)$ and the dimensionless group velocity $(1/c)(\partial\omega/\partial\alpha)$ vs x for typical value of the static magnetic field strengths. Again

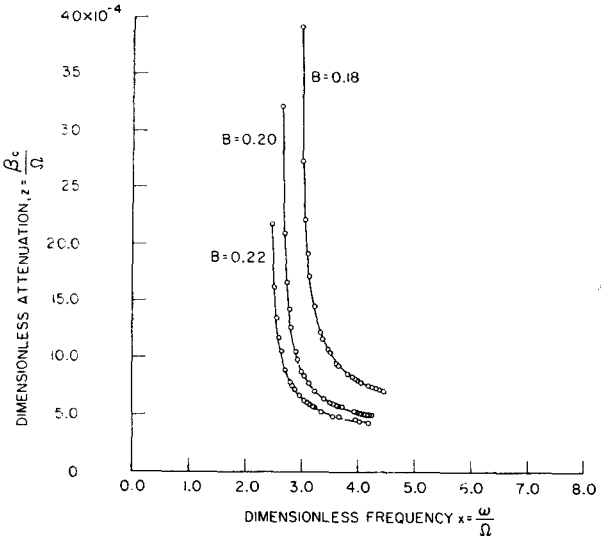

FIG. 4. Attenuation number versus frequency. The circles are experimental points, and the solid curve represents the best fit dispersion curve. Again B represents the axial magnetic field in webers per square meter.

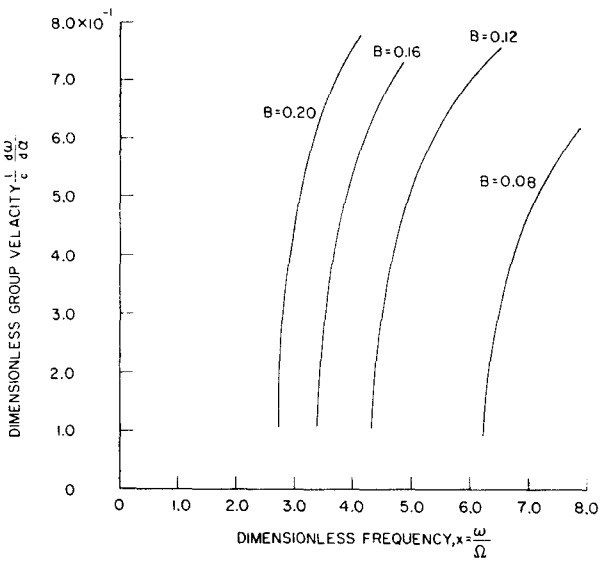

FIG. 6. Group velocity versus frequency. The continuous curves are taken from the dispersion relation. No experimental data were obtained for the group velocity.

the continuous curves represent the values of $(1/c)(\omega/\alpha)$ and $(1/c)(\partial\omega/\partial\alpha)$ as taken from the dispersion relation using the values of the five parameters appropriate to the value of B_0. In Fig. 5 the circles represent the normalized data points. The corresponding circles do not appear in Fig. 6 as no individual measurements of group velocity were made.

The results of the data analysis for $B_0 = 1$ kG is given in Table I. The measured values are taken from

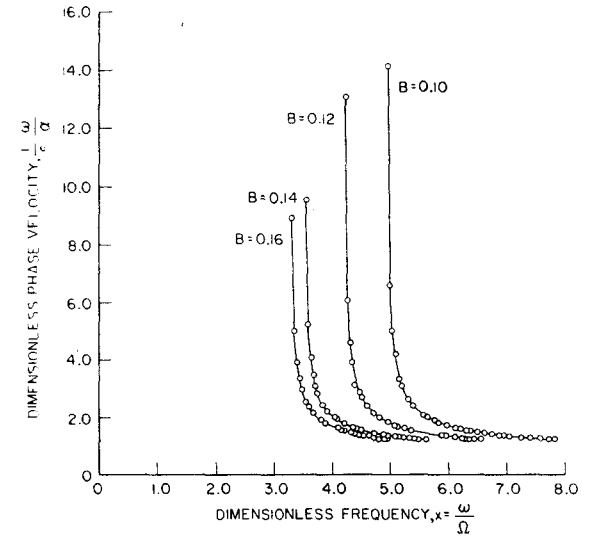

FIG. 5. Phase velocity versus frequency. Circles are normalized data points, and continuous curves are taken from the dispersion relation using values of the five parameters appropriate to the particular value of the axial magnetic field B.

independent determinations of the parameter[13–15] and the deduced values are the result of the data reduction.

Table II summarizes the ranges of values for the listed quantities derived from the present investigation. For the quantities above the dotted line (measured values except for group velocity), the limits are, in all cases, respective to the listed values of x. For the quantities below the dotted line (derived by least-squares adjustment of parameters), there is, of course, only one value for each field strength.

Figures 7–10 represent the general behavior of the dispersion function throughout the first quadrant of k, ω space. Plots are presented for $y = \alpha c/\Omega$ vs x, $z = \beta c/\Omega$ vs x, $(1/c)(\omega/\alpha)$ vs x, and $(1/c)(\partial\omega/\partial\alpha)$ vs x, respectively. The 1-kG magnetic field setting was typical, and these plots represent the dispersion

TABLE I. Result of data analysis for $B_0 = 1$ kG.

Parameter	Measured Value	Deduced Value
W	95.2 ms^{-1}	85.0 ms^{-1}
ν	(300 − 500)[a]	480 sec^{-1}
T_i	< 0.5 eV[13]	0.092 eV
l	15 mm	15.5 mm
δ	100 m^{-1}	102 m^{-1}

[a] Lower value obtained using viscosity data for argon.[14] Upper value obtained from measurements of Wobschall, Graham, and Malone.[15]

[14] E. H. Kennard, *Kinetic Theory of Gases* (McGraw-Hill Book Company, New York, 1938), p. 149.

[15] D. Wobschall, J. R. Graham, Jr., and D. P. Malone, Phys. Rev. 131, 1565 (1963).

TABLE II. Summary of the ranges of values for the listed quantities.

Quantity range	800 G	1600 G	2200 G
$x = \omega/\Omega$	6.12–7.96	3.32–4.96	2.48–4.20
Frequency (kHz)	187–243	202–303	208–352
Wavelength (m)	1.19–0.0458	0.341–0.0314	0.145–0.0248
Attenuation distance $\times$ $(\Omega/c) = 1/z$ (sec^{-1}	20–500	133–1110	455–2500
Phase velocity ($msec^{-1}$)	189 000–9060	65 500–9090	32 000-8720
Group velocity ($msec^{-1}$)	654–4510	726–5300	726–5810
Ion drift velocity W ($msec^{-1}$)	90.8	89.4	87.1
Effective ion collision frequency for momentum loss, ν (sec^{-1})	342.0	510.0	431.0
Ion energy, T_i (eV)	0.05	0.13	0.16
Radial cutoff distance, l, (m)	0.0152	0.0147	0.0152
Racial profile parameter, δ (m^{-1})	0.0100	0.0105	0.0105

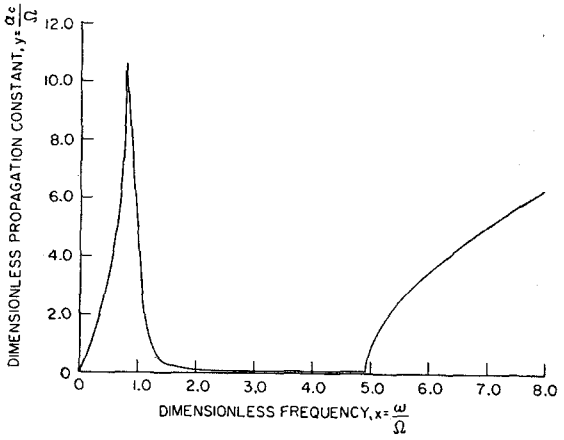

FIG. 7. Theoretical behavior of propagation number versus frequency for the first quadrant of k, ω space ($B = 0.1$ W/m^2). Experimental data were obtained for the right-hand curve only and are shown in Fig. 3.

function with the five parameters having values appropriate to that setting. Since the 1-kG data points have already been presented in some of the previous curves, these data are omitted in Figs. 7–10. Figures 7–9 are for the complete quadrant, but the group velocity is depicted only for the regions in which the damping is small, that is, where ion acoustic waves might be useful for communication purposes. These are the regions where $\partial\omega/\partial\alpha > 0$. In the regions of anomalous dispersion ($\partial\omega/\partial\alpha < 0$), the concept of group velocity becomes vague since it no longer represents the velocity of propagation of the signal.[16]

In the experiment the wave frequency was measured in the laboratory frame while the wavelength was measured in the plasma as it drifted antiparallel to the direction of propagation. Thus, W introduced a Doppler shift due to the moving medium, and the phase velocities were all slightly reduced by this effect.

Ion acoustic waves are produced by the Coulomb interaction (a long-range interaction). Propagation is possible only when the ion–neutral collision frequency is small compared with the wave frequency. The few collisions present tend to disrupt the long-range ordering, and damping increases with increasing collision frequency. Typical ion–neutral collision frequencies for this investigation were less than 500 sec^{-1}, so the condition of heavy damping would be encountered only at frequencies much less than those studied.

Ion–neutral collision decreased the wave phase velocity very slightly, but the more important effect was simply the introduction of a damping mechanism (and thus wave attenuation).

The effect of ion temperature is easily understood.

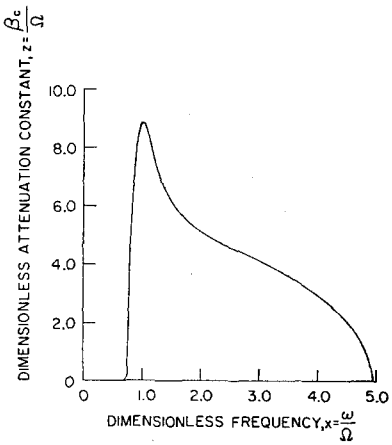

FIG. 8. Theoretical behavior of attenuation number versus frequency for the first quadrant of k, ω space ($B = 0.1$ W/m^2). It should be observed that the ordinate scale is much larger than that of Fig. 4 with the result that the attenuation number appears to go to zero for large values of x. Figure 4 gives the actual behavior for larger values of x.

[16] J. A. Stratton, *Electromagnetic Theory* (McGraw-Hill Book Company, New York, 1941), p. 339.

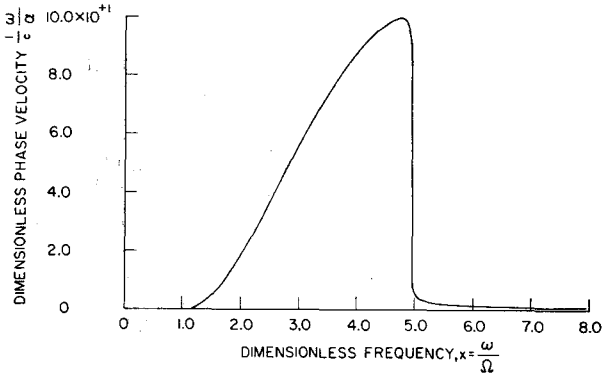

FIG. 9. Theoretical behavior of phase velocity versus frequency for the first quadrant of k, ω space ($B = 0.10$ W/m^2). The behavior for large values of x is in agreement with available experimental data. See Fig. 5.

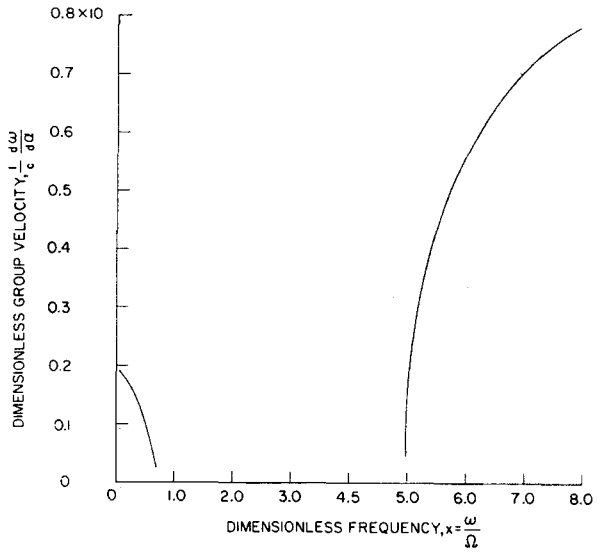

FIG. 10. Theoretical behavior of group velocity versus frequency for first quadrant of k, ω space ($B = 0.10$ W/m^2). The group velocity is depicted only where the damping is small, that is, where ion acoustic waves might be useful for communication purposes. See Fig. 8.

Since ion acoustic waves are density perturbations, they propagate at a velocity proportional to (pressure term/inertia term)$^{\frac{1}{2}}$. Passing from the case of cold ions to warm ions will increase the pressure term by a small amount equal to the ion pressure. Thus, the phase velocity will be slightly higher for a given frequency.

The primary effect of δ is to alter the form of the radial perturbation from J_0 to a more rapidly decreasing function of r. The effect of δ on y and z is a complicated second-order process; it will not be discussed further.

V. CONCLUSIONS

For the propagation of ion acoustic waves under conditions of negligible Landau damping, the dispersion relation derived in this paper is capable of predicting the propagation characteristics of the waves to within 10% (this is the greatest departure found between measured data and theory). The close agreement is probably attributable to the use of the unambiguous boundary condition that the perturbation extends a finite, measurable distance from the axis, rather than assuming the existence of a velocity or pressure node at the plasma boundary.

When damping processes other than ion–neutral collisions occur, the effective ion collision rate for momentum loss may be generalized to include these processes (such as the collision rate of ions with the walls of the container). In this case the effective collision frequency ν would be the sum of the individual collision rates for all processes. Electron momentum loss mechanisms may be ignored without appreciable error since negligible momentum is carried by the electrons.

The good agreement between measured and deduced values of the parameters W, l, and δ and the reasonable deduced values obtained for ν and T_i suggest the possibility that the externally accomplished excitation and dispersion measurements herein described could be a valuable diagnostic tool for the investigation of plasma characteristics, particularly when internal measurements (such as probe diagnostics) are impractical.

ACKNOWLEDGMENTS

We wish to thank Professor Kai Woehler, Professor A. W. Cooper, and Professor Elmo Stewart for many useful discussions. We are also indebted to Harold Herreman for his generous assistance in the laboratory and to Peter Wisler and Michael O'Dea for the construction of much of the equipment used in the experiment. Deepest appreciation also goes to Robert Hilliary for giving generously of his time and ability in the preparation of the computer programs so vitally necessary for the reduction and analysis of the experimental data.

This work was begun at the Naval Postgraduate School (and supported by the Office of Naval Research) and completed at the Department of Nuclear Engineering and the Research Laboratory of Electronics, Massachusetts Institute of Technology [work supported by the United States Atomic Energy Commission under Contract AT(30-1)-3285].